GEMINI
8-M Telescopes
Project

RPT-O-G0001

Theoretical Study of the Image Quality of an 8M Primary Mirror Having Print-through Undulations over the Mirror Surface

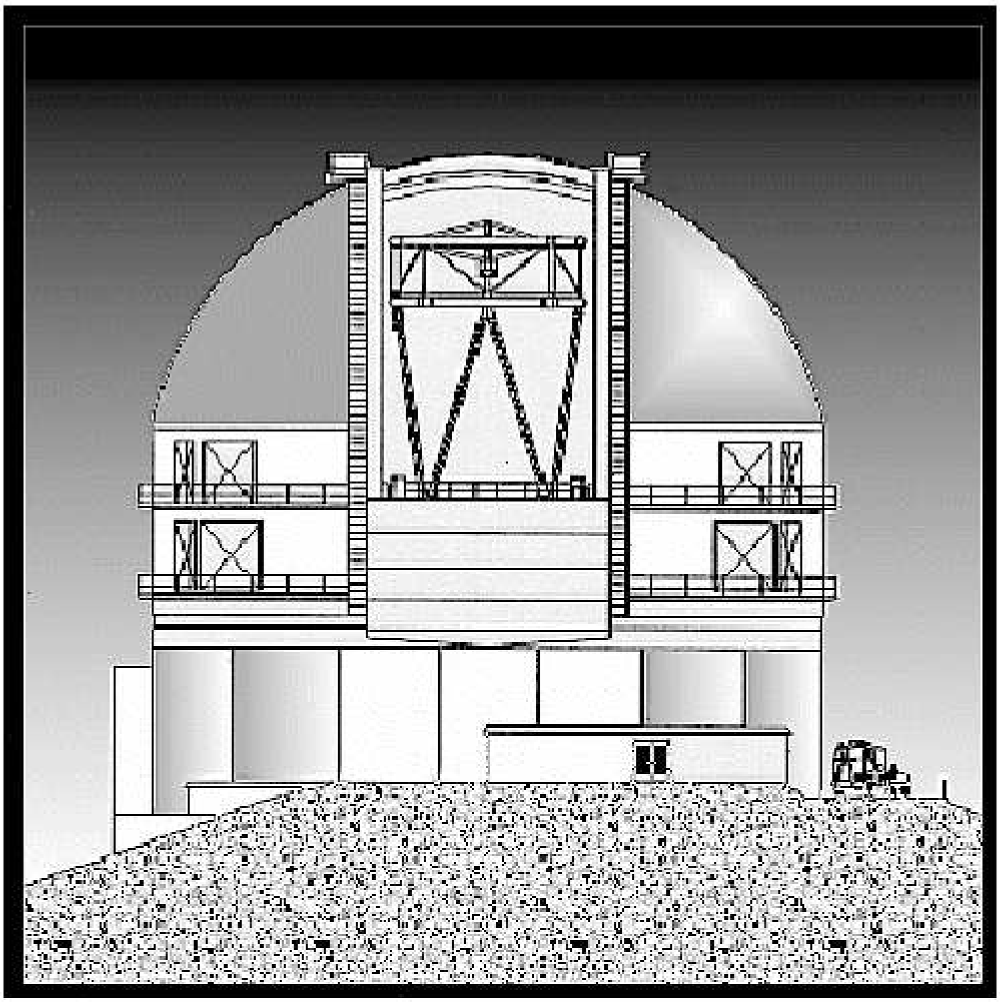

G Catalan, C M Humphries and E Atad-Ettedgui
Royal Observatory Edinburgh

December 1991

GEMINI PROJECT OFFICE 950 N. Cherry Ave. Tucson, Arizona 85719
Phone: (520) 318-8545 Fax: (520) 318-8590

CONTENTS

1. Description of evaluation programme

Optical fabrication of large astronomical honeycomb mirrors results in the formation of "print-through" undulations over the mirror surface. In response to a request from the Gemini 8m Telescope Project for evaluation of the effect of print-through on image quality, the following analysis was performed.

The undulations were assumed to be distributed regularly over the surface, with height variations z defined[l] relative to the parent paraboloid by

$$z - A\cos^2\left\{\frac{\pi}{c}x - \frac{\pi}{\sqrt{3}c}y\right\}\cos^2\left\{\frac{2\pi}{\sqrt{3}c}y\right\} \qquad (1)$$

where A is the peak-to-valley amplitude, and c is the centre-to-centre spacing, taken to be 20 cm. A portion of the surface contours resulting from this hexagonally packed function is shown in Figure 1. The diffraction structure and relative intensities were calculated for two values of amplitude A, 50 nm and 20 nm, and three values of wavelength, 350 nm, 633 nm and 2200 nm. A structure function relating the RMS surface height differences and the separation of sampled points was derived analytically.

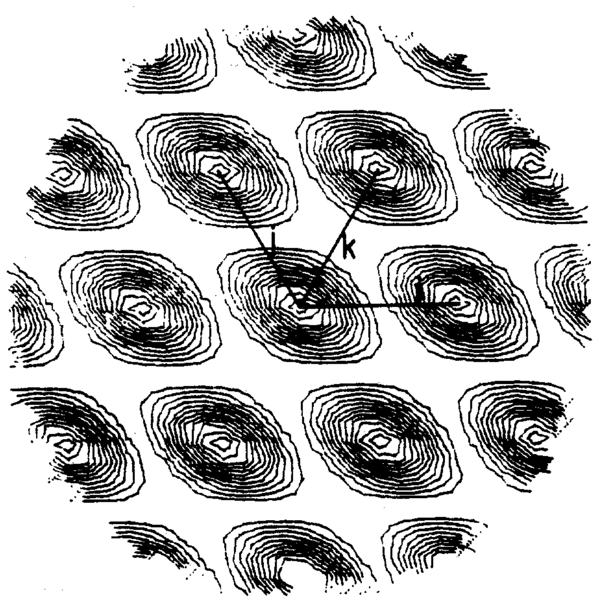

Figure 1. Portion of the contour plot of $(\text{cosine})^2$ surface function

An earlier investigation of the same effect based on a square distribution of bumps giving a Strehl ratio of 0.97 at $\lambda = 3\mu m$, including random height variations, was also undertaken and the results of this are presented in Section 4.

2. Diffraction structure and intensities: hexagonal pattern print-through

In order to sample at sufficient resolution each of the approx. 1250 bumps of an 8m mirror the surface deformations were described by a 500 x 500 matrix in the interferometric file of CODE V. The computations consisted of (a) ray tracing, (b) evaluation of the pupil phase map, and (c) calculation of a 512 x 512 array of PSF values at points separated by intervals of $\lambda F/2$ (where F = 1.8 is the focal aperture ratio).

(a) Diffraction pattern for amplitude A = 20 nm p-v

The PSFs for an amplitude of 20 nm at λ = 350, 633 and 2200 nm are presented in Figure 2 with both linear and logarithmic intensity scales. The logarithmic scale encompasses five decades in each case. The plots are essentially the diffraction patterns of a two-dimensional phase grating, with side peaks located at angular distances of $\lambda/(\sqrt{3}c/2)$ from the central peak corresponding to the separation $\sqrt{3}c/2$ between adjacent rows of bumps, or multiples thereof. Table 1 shows the positions of the innermost peaks due to the surface undulations and compares these with the radii of the first diffraction rings around the Airy discs for unaberrated systems.

Table 1: Radial positions of innermost image peaks

λ(mm)	Radii of circles containing innermost image peaks	
	Structured 8m mirror	Unaberrated 8m system (1st diffraction ring)
350	0.42 arcsec	0.009 arcsec
633	0.75	0.016
2200	2.62	0.057

Since with A = 20 nm even the strongest side peaks in Figure 2 have intensities no more than 1% of the central peak intensity, the linear plots are relatively featureless. In the logarithmic plots the strongest side peaks have intensities that vary between 1% (at λ = 350nm) and 0.02% (at λ = 2200nm) of the central peak intensity of an unaberrated system. That the intensities of the peaks in Figure 2 are enhanced preferentially along the direction $y = \pm\sqrt{3}x$ is a consequence of diffraction from the rhomb shaped (instead of rotationally symmetric) unit cells given by equation (1) and shown in Figure 1. For comparison, the PSF structure of an unaberrated system for λ = 633 nm is shown in Figure 3 where all diffraction rings with intensities higher than 10^{-5} of that of the central peak are contained within a radius of 0.35 arcsec.

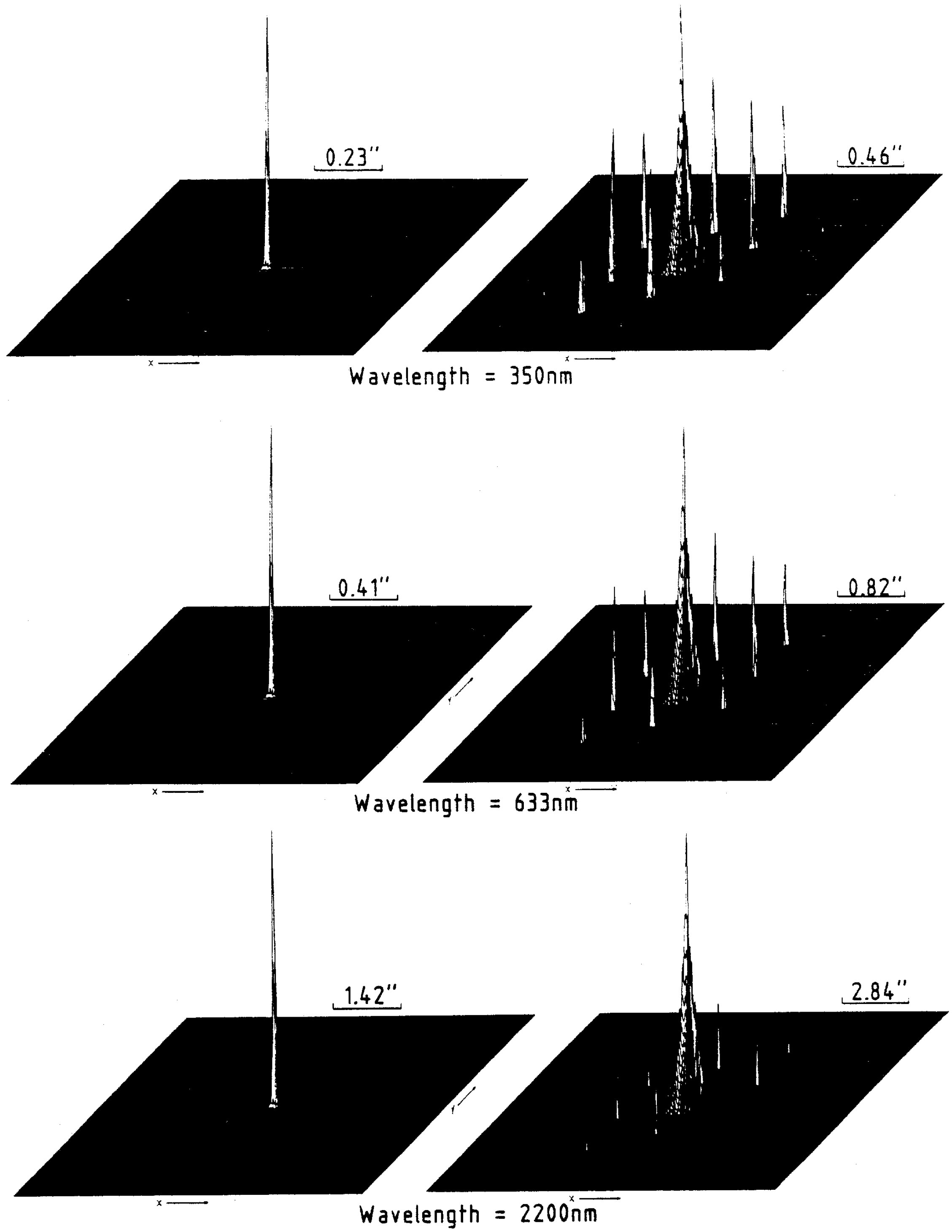

Figure 2. PSFs for an 8m mirror with surface undulations of amplitude 20 nm p-v at three wavelengths. The vertical intensity scales shown on the left are linear whilst those on the right are five decade logarithmic.

Table 2 summarizes the strongest individual side peak intensities relative to the central peak of an unaberrated system, together with the corresponding single side peak energies and the Strehl ratios. Also shown are the stellar magnitude differences between the strongest side peak and the central peak, together with the total fractions of energy re-distributed from the central peak of an unaberrated system into all of the side peaks combined. The magnitude differences quoted here assume that the detector pixel resolution is such that the total energy within a peak, rather than the central intensity, is the appropriate quantity to be compared. The RMS wavefront errors given in Table 2 were determined analytically as described in Section 3. Encircled energy plots are given in Figure 4. These extend over an area around the main peak with dimensions several times that of the Airy disc. Numerical data are given in Table 3.

Table 2: Intensities of diffraction structure for A = 20 nm

Wavelength (nm)	350	633	2200
Strongest side peak intensity	$1.0\ 10^{-2}$	2.010^{-3}	$1.6\ 10^{-4}$
Strehl ratio	0.96	0.99	1.00
Strongest side peak energy	$4.6\ 10^{-3}$	$1..8\ 10^{-5}$	$1.2\ 10^{-4}$
Magnitude difference	10.8	11.9	14.8
Total side peak fractional energy	0.15	0.11	0.09
RMS wavefront error velengths)	0.032	0.018	$5.1\ 10^{-3}$

Table 3: Encircled energy diameters (arcsec) for A=20nm

Wavelength (nm) Energy Percentage	350	633	2200
50	0.011	0.019	0.066
60	0.013	0.022	0.077
70	0.015	0.026	0.089
80	0.024	0.035	0.115
90	0.059	0.082	0.239
94	0.159	0.146	0.419

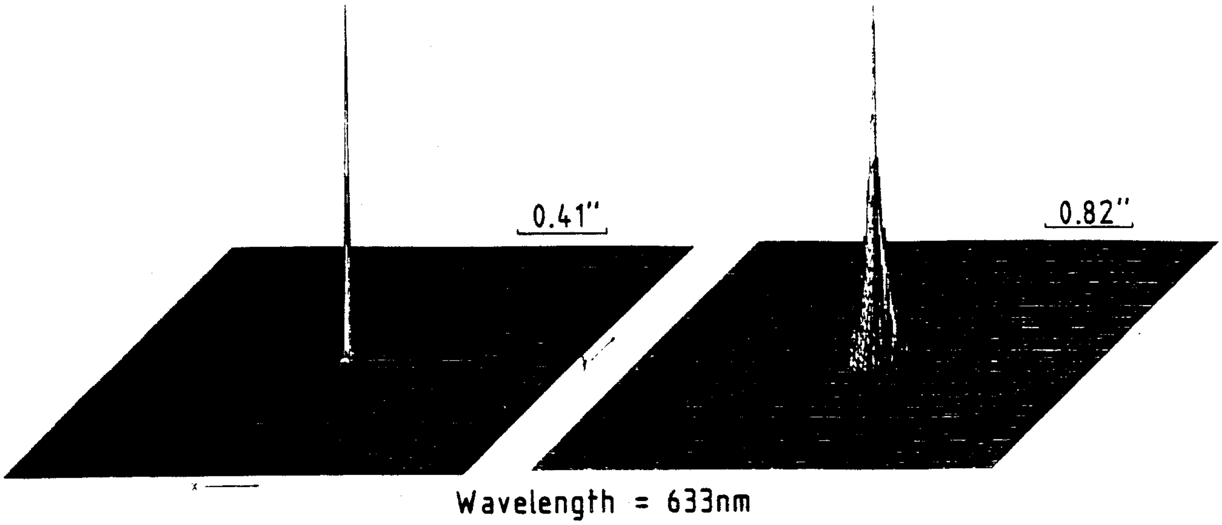

Figure 3. PSF structure of an unaberrated system shown on linear (left) and logarithmic (right) intensity scale.

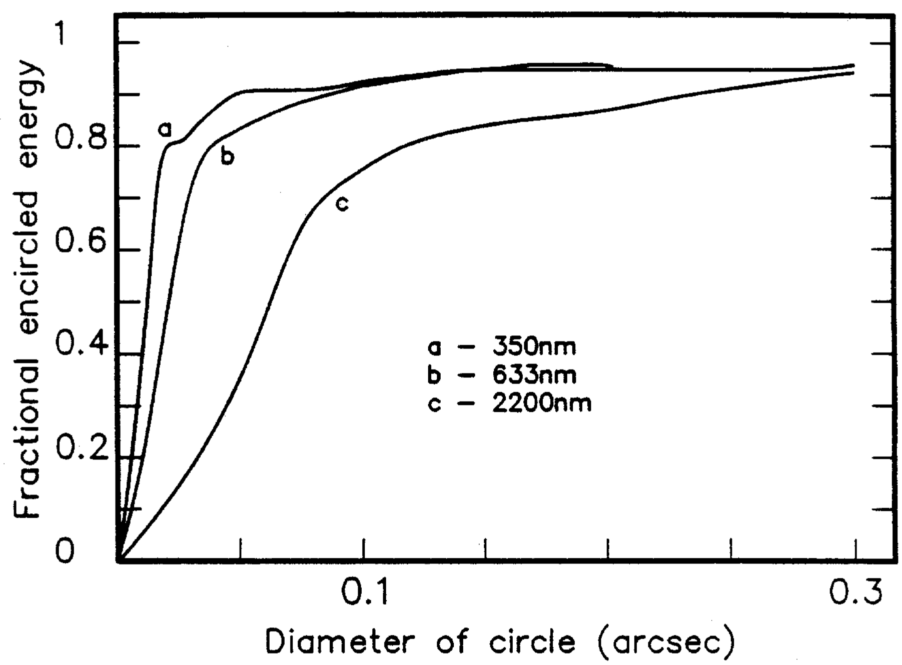

Figure 4. Encircled energy plots for amplitude A = 20 nm p-v

(b) Diffraction pattern for amplitude A = 50 nm p-v

The structure described above for A= 20 nm is relatively weak. For example, the stellar magnitude differences between the main peak and the strongest side peaks are greater than 10. For this reason, instead of investigating the effect of smaller amplitudes (e.g. A = 5 or 10 nm) it was considered of more interest to take for comparison a higher value of A. It was decided to use A = 50 nm p-v since for the worst case at the shortest wavelength (λ = 350 nm) this gives a Strehl ratio of 0.79, i.e. it is still just about diffraction limited by the Strehl criterion.

Figure 5 shows the PSFs on linear and logarithmic intensity scales. In this case, as much as 25 % of the incident energy may be redistributed into the diffracted side peaks (whereas for A = 20 nm the corresponding amount is less than 10%). Table 4 gives the intensity and energy data of the side peaks and Figure 6 shows the encircled energy diameters. At the shortest wavelength the strongest diffracted peak has 3 % of the intensity of the central peak. Numerical data for the encircled energy diameters are presented in Table 5.

Table 4: Intensities of diffraction structure for A = 50 nm

Wavelength (nm)	350	633	2200
Strongest side peak intensity	3.10^{-2}	1.10^{-2}	1.10^{-3}
Strehl ratio	0.79	0.93	0.99
Strongest side peak energy	$3.3\ 10^{-2}$	$1.4\ 10^{-4}$	$9.0\ 10^{-6}$
Magnitude difference	3.7	9.6	12.6
Total side peak fractional energy	0.29	0.17	0.10
RMS wavefront error (wavelengths)	0.08	0.044	0.013

Table 5: Encircled energy diameters (arcsec) for A =50 nm

Wavelength (nm)/ Energy Percentage	350	633	633 (aberration-free system)
50	0.014	0.020	0.019
60	0.019	0.023	0.022
70	0.033	0.029	0.026
80	0.25 (78%)	0.053	0.033
90	--	0.212	0.068

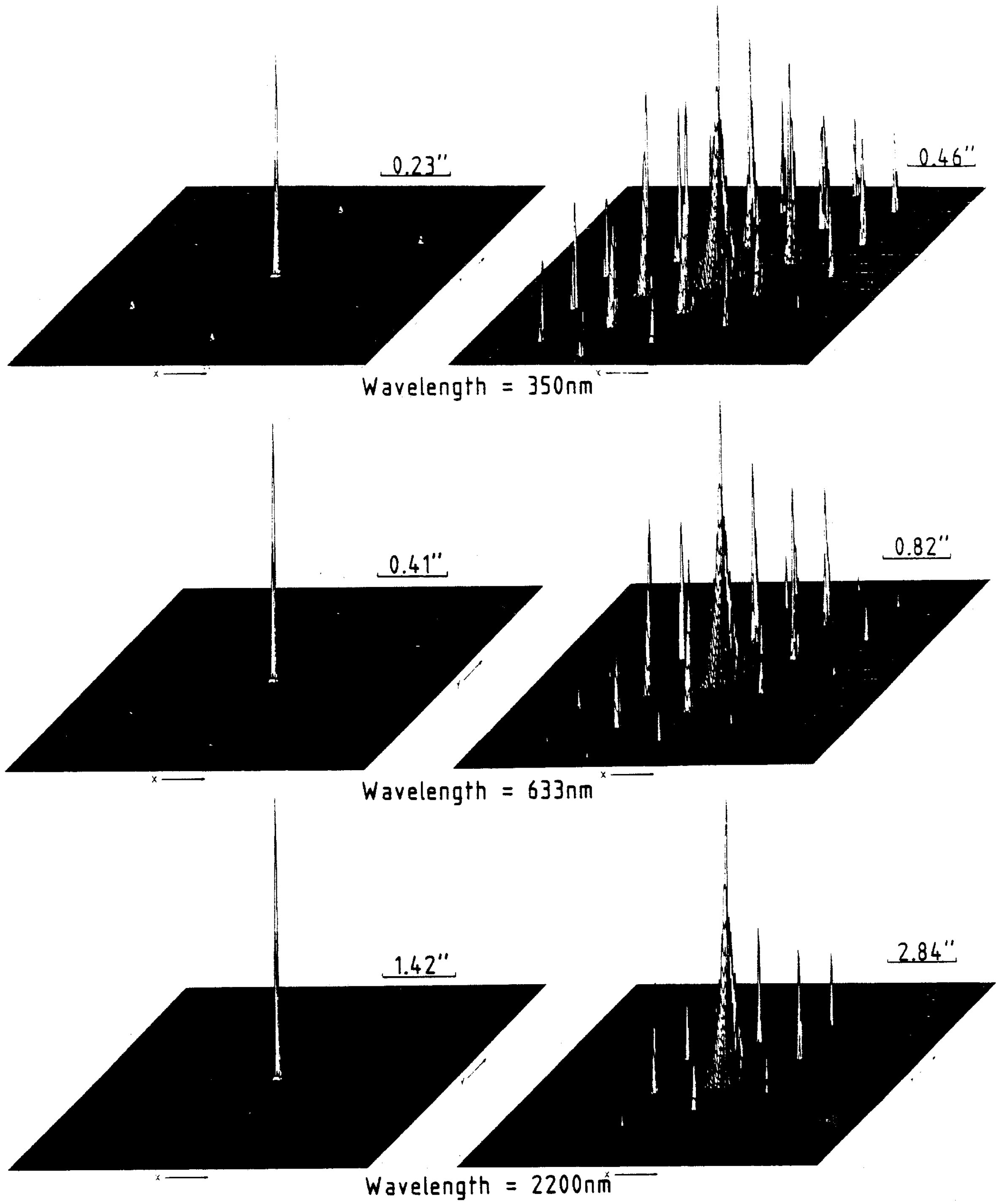

Figure 5. PSFs for an 8m mirror with surface undulations of amplitude 50 nm p-v at three wavelengths, shown on linear and logarithmic intensity scales.

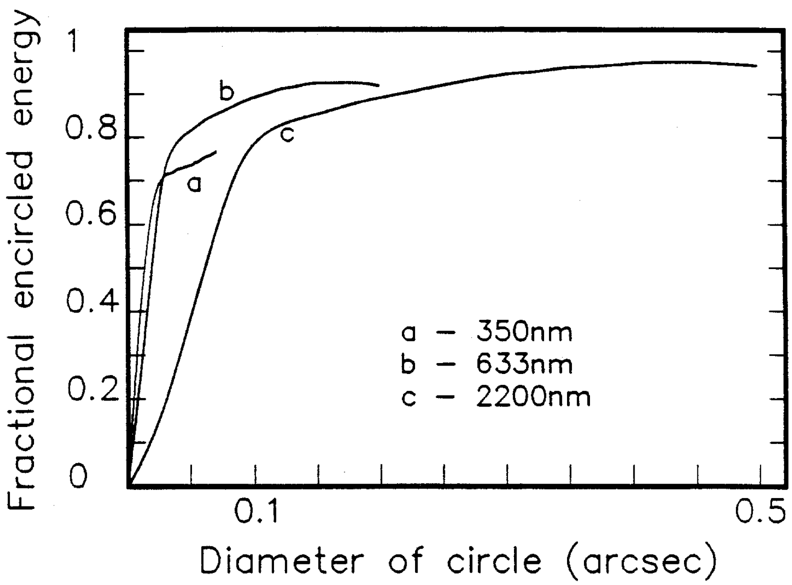

Figure 6. Encircled energy plots for amplitude A = 50 nm p-v

3. <u>Analytic derivation of structure function</u>

By analogy with the atmospheric phase structure function defined by the variance of the phase,

$$D_{\phi}(\Delta r) = <[\phi(r) - \phi(r + \Delta r)]^2 > \tag{2}$$

we may similarly define a surface height structure function given by

$$D_z(\Delta r) = <[z(r) - z(r + \Delta r)]^2 > \tag{3}$$

Here $D_z(\Delta r)$ is the square of the RMS height variation σ_z along a specified direction over the surface of the mirror; z is given by expression (1); and the spatial average < f > of the periodic function f is $\int_o^c f dr / \int_o^c$ for the period c. In our case c is the centre-to-centre spacing of the surface undulations. Applying expression (3) to the surface shape given by (1), we find

$$\sigma_z^i(\Delta r) = \sigma_z^j(\Delta r) = \frac{A}{\sqrt{2}} \left| \sin\left(\frac{\pi}{c}\Delta r\right) \right| \tag{4a}$$

$$\sigma_z^k(\Delta r) = \frac{A}{\sqrt{2}} \left[1 + 0.25\cos^2\left(\frac{\pi\Delta r}{c}\right)\right]^{1/2} \left| \sin\left(\frac{\pi\Delta r}{c}\right) \right| \tag{4b}$$

where i, j and k are the directions along the centre lines shown in Figure 1. The structure functions given by 4(a) and 4(b) are plotted in Figure 7. The periodic shapes of these curves follow from the periodicity contained in expression (1). In practice, random amplitude errors are likely to reduce the depth of the minima that occur at multiples of 20cm.

The RMS surface deformation over the mirror area, equal to the RMS deformation over the unit cell of Figure 1, was obtained as a fraction of the peak-to-valley amplitude A by integration of (1) as

$$\sigma_2 = 0.28A$$

The RMS wavefront errors in Tables 2 and 4 are twice the RMS surface errors σ_z given by (5).

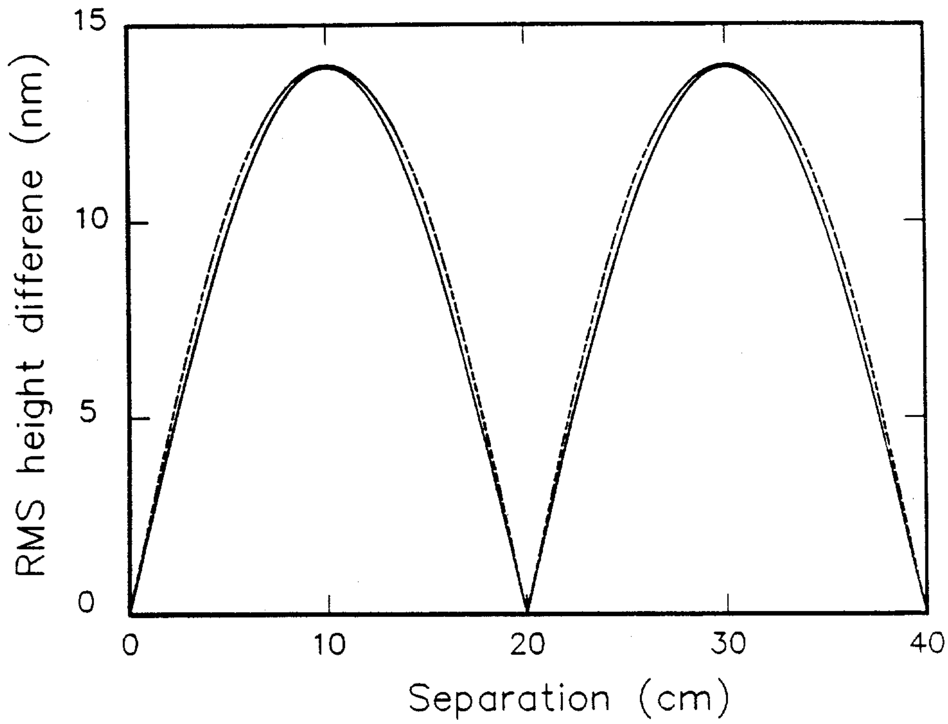

Figure 7. Surface deformation structure functions given by equations 4(a), solid line, and 4(b), dashed line.

4. Diffraction structure and intensities: square array print-through

(a) Uniform amplitude

An earlier analysis of the image structure was based on a square array of sinusoidal bumps with deformation z given by

$$z = \frac{A}{2}\cos\left(2\pi\frac{x}{c}\right)\cos\left(2\pi\frac{y}{c}\right) \tag{6}$$

where the peak-to-valley amplitude A was chosen to give a Strehl ratio S = 0.97 at λ = 3 lim [2]. Using the approximation

$$S = 1 - \left(\frac{2\pi\sigma}{\lambda} \right)^2 \tag{7}$$

where the wavefront RMS value σ is twice the surface RMS deformation σ_z, this corresponds to an RMS value σ_z = 41.3 nm. Integration of (6) over a unit cell gave the relationship between peak-to-valley and RMS amplitudes as

$$\sigma_z = 0.25A \tag{8}$$

leading to the value A = 165 nm. A contour plot of a portion of the surface structure is shown in Figure 8. That the amplitude here is so much larger than that used for the hexagonal print-through is unfortunate (since it reduces the possibility of making comparisons of the results due to different geometries) but arises wholly from the proposed Strehl value requirement at λ = 3µm. It could not be reduced without changing the underlying basis of the specification proposed at that time.

Table 6 presents the Strehl ratios, RMS wavefront errors, and the strongest single side peak intensities relative to the central peak intensity of an unaberrated system for each of the wavelengths considered. As is evident from Table 6 the Strehl ratio decreases rapidly towards shorter wavelengths and, despite the apparently tight Strehl specification for λ = 3µm, the optical performance in the short wavelength visible and ultraviolet would be regarded as unacceptable for many purposes. The PSF at λ = 633 nm is shown in Figure 9; here the side peaks on the x = 0 and y = 0 directions do not appear because the minimum of the diffraction pattern from a single bump happens to coincide with the maximum of the diffraction pattern from the array. However, the strongest side peaks have 7% of the intensity of an unaberrated central peak.

Table 6: Intensities of diffraction structure for a uniform amplitude square print-through array

Wavelength (nm)	350	633	3000
Strongest side peak intensity	7×10^{-2}	7×10^{-2}	-
Strehl ratio	0.10	0.53	0.97
RMS wavefront error (wavelengths)	0.24	0.13	0.03

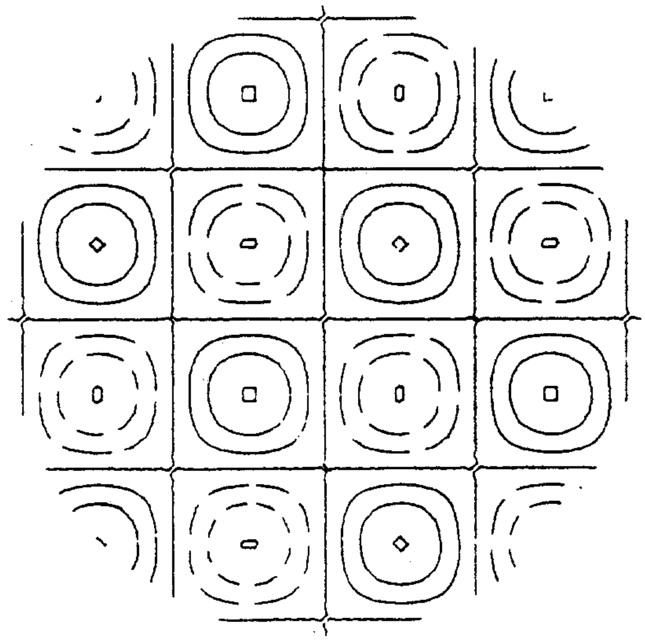

Figure 8. Portion of contour plot for cosine surface function with uniform amplitude.

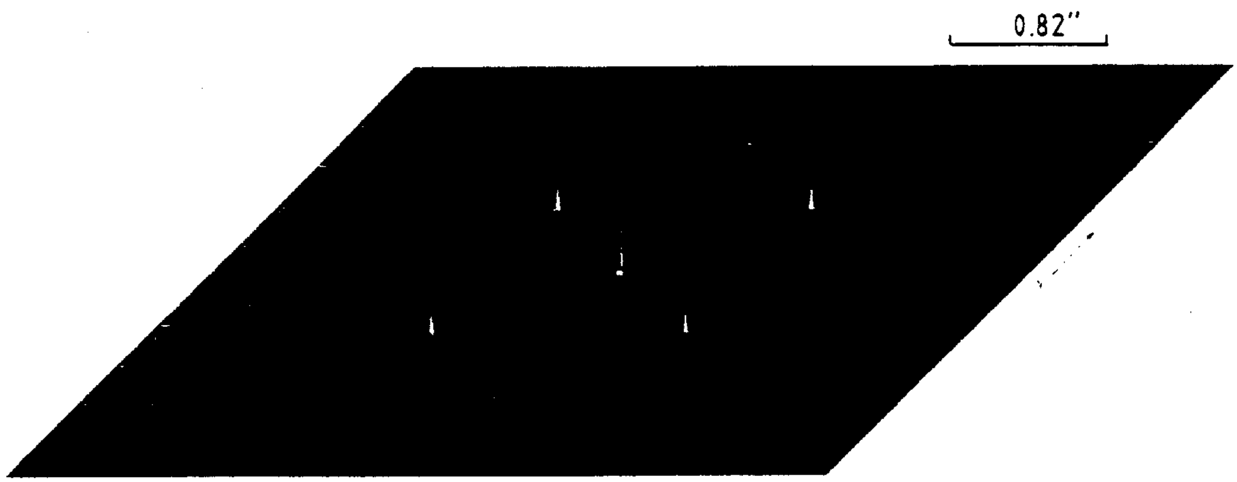

Figure 9. PSF for a square array of surface undulations at wavelength 633 nm; linear intensity scale.

(b) Random amplitude

The effect of print-through undulations over the mirror surface that have randomly sized amplitudes were investigated by considering the deformation z, of an individual bump to be

$$Z_i = \frac{A_i}{2}\cos\left(\frac{\pi x}{c}\right)\cos\left(\frac{\pi y}{c}\right) \tag{9}$$

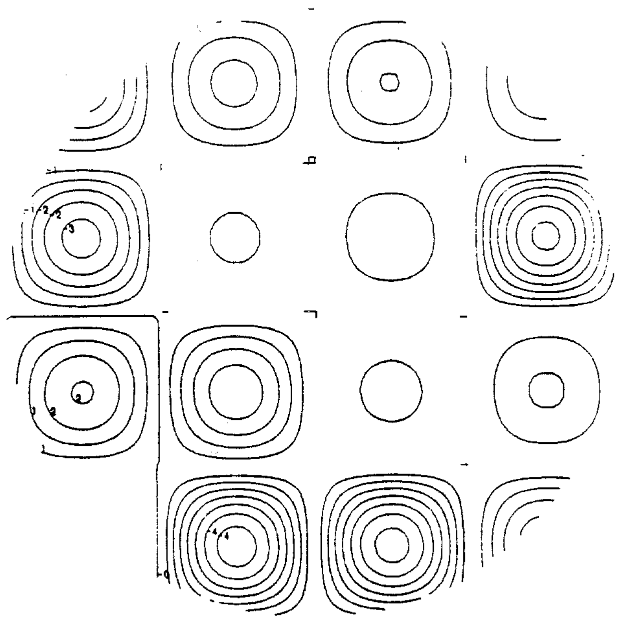

Figure 10. Contour plot of cosine surface function with randomly sized amplitudes.

A contour plot of this function is given in Figure 10 and cross-sections along the x direction are compared in Figure 11 for the functions given in equations (6) and (9). For (9), the A_i were derived by a random number generator with a uniform probability distribution and with surface deformation limits set between ± 143 nm. The latter value was chosen to give the same RMS wavefront deformation as for the uniform amplitude case, and hence the same Strehl ratio at λ = 3μm.

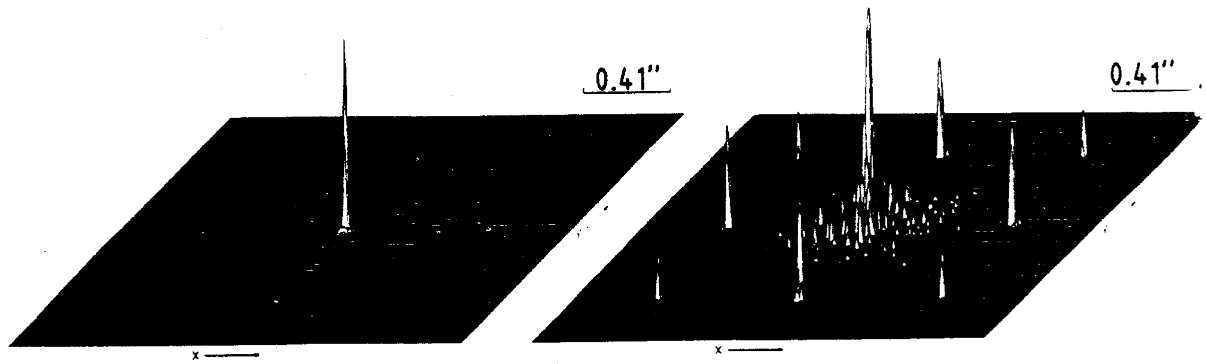

Figure 12. PSF for a square array with random amplitudes (a) linear, and (b) logarithmic intensity scale with three decades. Wavelength 633 nm.

The effect of these random amplitude deformations on the diffraction structure of the image is summarized in Table 7 and shown in Figure 12. Whereas for the uniform amplitude square array the strongest side peaks are located along the x = ±y diagonals, the strongest side peaks of the random amplitude array now lie on the x o and y = o axes. The latter are also much weaker.

Also evident in Figure 12 is the appearance of low intensity, densely packed, "grass" around the central peak. At even lower intensities, this weak structure extends over the whole field examined. As the RMS wavefront error σ becomes increasingly larger at short wavelengths, so the Strehl ratio is no longer related simply to σ; thus, the differing values of S at λ = 350nm in Tables 6 and 7 result from a dependence also on the distribution of amplitudes across the array. Repeat calculations of the random amplitude case gave small variations in the intensity distributions of the low intensity grass and variations also in the resulting Strehl values. Note

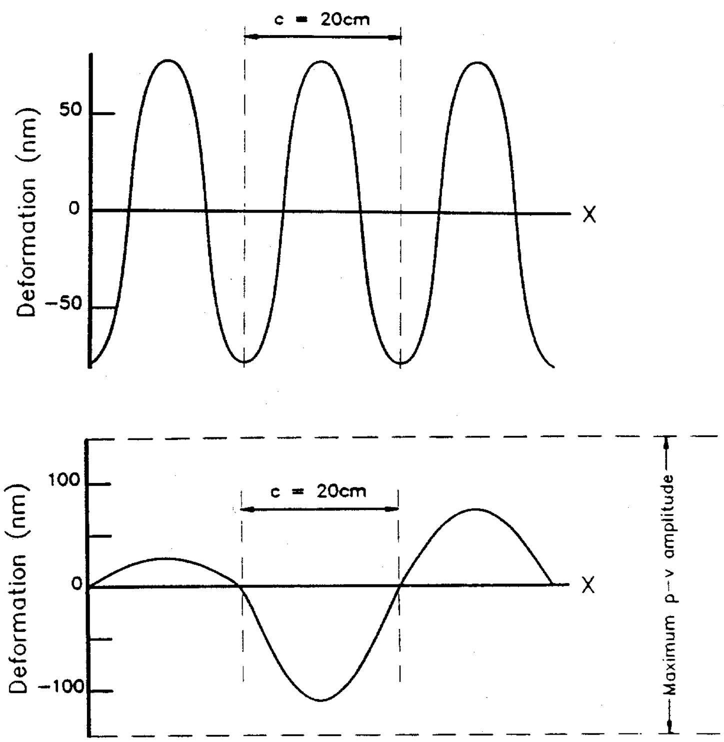

Figure 11. Cross-sections of surface undulations defined by equations (6) and (9).

that the Strehl ratios in Tables 6 and 7 for λ = 350 and 633nm are the values obtained by the full diffraction calculations and not from approximate formulae.

Table 7: Intensities of diffraction structure for a random amplitude square print-through array

Wavelength (nm)	350	633	3000
Side peak intensity ratio	4×10^{-2}	1×10^{-2}	--
Strehl ratio	0.21	0.54	0.97
RMS wavefront error (wavelengths)	0.24	0.13	0.03

5. Summary of main conclusions and other comments

5.1 Print-through structure on a mirror behaves optically as a two-dimensional phase grating. The pattern and intensities of peaks in the associated image structure can be determined by Fraunhofer diffraction calculations with the pupil function modified to incorporate phase variations produced by the printthrough. This can be done either by theoretical modeling, as is the case in this Report, or by experimentally determined profiles.

5.2 The innermost side peaks in the structure of such images occur at radii of many multiples of the diffraction ring radii for an unaberrated system. For hexagonal pattern print-through with amplitudes of 20nm p-v, the strongest individual side peaks have intensities at short wavelengths of 1% of that from the central peak of an unaberrated system. In terms of total energy, as much as 15% of that from an unaberrated system may be diffracted into the pattern of side peaks, with the strongest side peak differing in energy from an unaberrated central peak by 10.8 stellar magnitudes (with λ = 350nm and A = 20nm). This is despite such systems being well diffraction limited in terms of the Strehl criterion. The corresponding data for A = 50nm are given in Table 4.

5.3 The structure function (Figure 7) for periodic mirror undulations given by equation (1) with uniform amplitude show perfect correlation at intervals equal to the centre-to-centre spacing. An experimentally determined structure function for the 3.5m WIYN mirror[3] indicates that real mirrors do not exhibit such perfect correlation; in practice, therefore, random amplitudes and/or variable centre-to-centre spacings may modify the structure function.

5.4 The results of diffraction calculations for a square array print-through given in Section 4, and based on a proposed specification of Strehl ratio s = 0.97 at λ = 3μm, lead to large wavefront error amplitudes at visible and UV wavelengths and to high side peak intensities and low Strehl ratios. Such a specification is not suitable for a short wavelength diffraction limited system.

5.5 With a square array of mirror undulations of random amplitude the centre-tocentre spacings remain the same and the main diffraction peaks still form regular pattern along the axial directions and the diagonals. The effect of the random bump heights is to lower the intensity of the main side peaks and to produce low intensity "grass" around the central peak. A more realistic set of calculations would be based on having random amplitudes where the randomness is restricted between tighter limits than those used here.

5.6 The image structures presented in this Report have been calculated for monochromatic inputs. For broadband applications it should be remembered that the image structure will be smeared out according to the bandwidth.

6. Acknowledgements

The work described in this Report was undertaken by the Applied Physics Section at the Royal Observatory, Edinburgh, as part of its contribution to the Gemini Project development programme. The support of Larry Stepp (Gemini Optics Manager, Tucson) and of Roger Davies (UK Gemini Project Scientist) are gratefully acknowledged. Gavriel Catalan's involvement was made possible by a period of sabbatical leave from Israel.

7. References

1. Pearson, E., NOAO Memorandum, 20 September 1991.

2. Stepp, L., Proposal for Theoretical Study, Gemini Project, Tucson, 20 June 1991.

3. Stepp, L., Data presented at Gemini meeting, Durham, June 1991.